Computing and Informatics, Vol. 32, 2013, 1117–1130

AUTONOMOUS TAKEOFF AND LANDING CONTROL FOR SMALL SIZE UNMANNED AERIAL VEHICLES

Dániel Stojcsics, András Molnár

John von Neumann Faculty of Informatics
Óbuda University
Bécsi út 96/b
1034, Budapest, Hungary
e-mail: {stojcsics.daniel, molnar.andras}@nik.uni-obuda.hu

Abstract. The aim of the research was to develop an Unmanned Aerial Vehicle (UAV) hardware and software which can control a small size UAV (with 1–10 kg takeoff weight) from takeoff to landing. The research was based on AERObot V5 autopilot, developed and tested previously by us. AERObot can control a chosen aerial vehicle on a predefined route and altitude reliably but requires manual takeoff and landing. The speciality of the new takeoff and landing methods is that they do not need any additional RF guidance transmitter, onboard radio/ultrasonic altimeter or special navigation marker points. Using only the existing onboard sensors (GPS, Inertial Measurement Unit – IMU, barometric airspeed meter, barometric altimeter) AERObot can safely take off and land the UAV under the specified weather limitations for the aerial vehicle frame.

Keywords: Unmanned Aerial Vehicle, UAV, HIL simulation, test flight, takeoff, landing, approach, flare, navigation, vector field, ILS

1 INTRODUCTION

The developement of the fully automatic system was done to meet several criteria. The flight was split into three well specified parts. These are the takeoff, waypoint navigation (mission) and the landing. The main difference between them is that they are using different control laws and methods. The reason for this is that different parts require different control precision of flight parameters. Switching between the flight modes requires transientless transition. Since the used UAVs are small-size, it

is impossible to use similar or same onboard RF guidance receiver systems like ILS, which are used generally in commercial aviation. Another aim was to prevent the usage of any additional ground device during takeoff and landing. The method must operate in the simplest way even on a plain grass field without any easy-to-recognize runway elements (concrete runway, centerline markers, etc.) Regarding the complexity the method was first tested separately and then combined in Hardware-In-the-Loop simulation using Matlab/Simulink. The advantage of this simulation is that it can reveal software and algorithmic errors since the whole control and navigation runs onboard. Since the simulation was precise the used parameters for real test fligts were the same, only minor fine tuning was necessary. The Takeoff command sets the takeoff direction and enables the engine. The UAV climbs in a safe angle with full throttle, then switches to waypoint navigation, climbing towards the flight level.

After completing the mission the UAV approaches the landing zone. It can be the same as the takeoff place or can be different. When it is not the same, manual waypoint editing is required, otherwise it is calculated onboard based on home position and the used takeoff direction. After approaching the UAV performs the glideslope ($-10°$) path following maneuver at 30–100 m altitude. Then, at 5–10 m altitude it performs the flare, slowing the descent rate just before touchdown, and stops the engine.

2 INSTRUMENT LANDING SYSTEM

Instrument Landing System is a highly accurate and dependable ground based instrument approach system for general aviation. The system consists of radio signal transmitters and lighting arrays on the ground and radio signal receivers onboard [1, 2]. The localizer is a VHF radio transmitter and antenna system, usually located at the end of the runway. Two signals are transmitted using the general range of VOR transmitters (between 108.10 MHz and 111.95 MHz). One is modulated at 90 Hz, the other at 150 Hz. The overlap between the two areas provides the on-track signal. The glide slope provides vertical guidance (Figure 1) during the approach using another antenna array on one side of runway. ILS marker beacons provide distance information from the runway by identifying predetermined points (outer, middle, inner marker) along the approach track.

There are many lighting systems to aid landing: approach light system (ALS), sequenced flashing light (SFL), touchdown zone lights (TDZ) and centerline lights. Since ILS is used by commercial aviation at airports it cannot be used as a general guidance system for UAVs, since there are no ground instruments on an ad-hoc UAV airfield, and the onboard part is way too heavy and big for a small size aerial vehicle.

3 HARDWARE IN THE LOOP SIMULATION

The HIL simulation is able to create the same environment as the real flight. The autopilot is acting the same as real; it has no information about the source of the

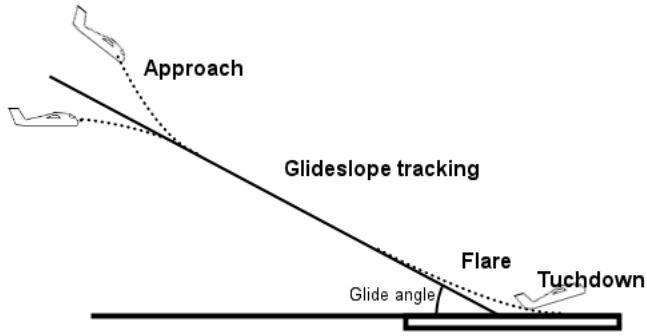

Figure 1. Instrument landing system – glide slope

measured signals which are generated with PC simulation software. A mathematical model, created in Matlab/Simulink, processes the states of the UAV using the actuator signals captured from the autopilot. The autopilot is using the simulated signals instead of its own internal sensors for the filter, navigation and control algorithms. The simulator sends the output of the simulation (position, orientation, airspeed and altitude etc.) to the autopilot via serial port with a desired control frequency (e.g. 100 Hz) which is the same as the update frequency of the control functions (discrete time simulation with a real time model). The autopilot is not using its internal timer but the timestamp from the simulator. The simulated outputs can be ideal or noisy (generated). Using ideal values the internal filters can be bypassed. Otherwise the HIL simulation is capable of testing the onboard software filters in different situations. The autopilot calculates and sends back the actuator signals based on the received values while also refreshing the physical actuator. These signals are the inputs of the simulation model. The generic small size fixed wing UAV model was created in Matlab/Simulink using the AeroSim block set using a predefined UAV 6-dof model for the validation purposes of the HIL simulation (Figure 2). Considerable amount of conclusion and test data is available for the control functions and navigation from real flights in the past, so the simulated results could be compared to real measured ones. The selected block set has an interface to FlightGear flight simulator so the HIL test flights can be observed in such a graphical way. The takeoff, waypoint flight and landing procedures were tested using this method (Figure 3) [3].

4 IN-FLIGHT NAVIGATION

The base sensor for the navigation is the GPS. It provides the position, speed over ground (SOG), bearing and many other parameters used by the navigation algo-

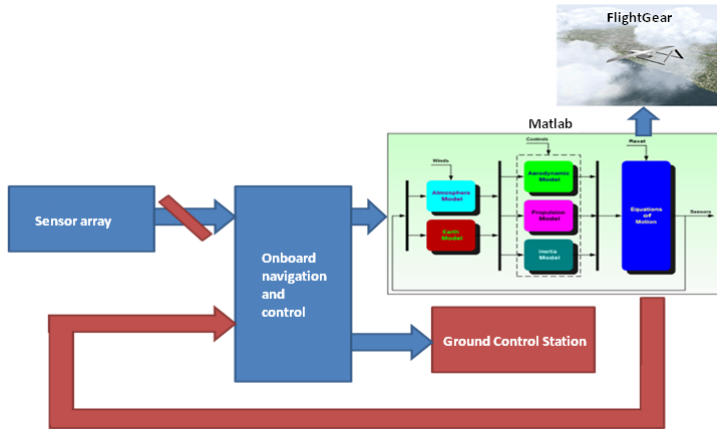

Figure 2. HIL simulation

rithms. The maximum position refresh rate of best GPS modules is about 5–10 Hz, which is not enough for precision flight control. The other problem is the refresh rate is not reliable because NMEA sentences and the checksums are often incorrect. AERObot is using waypoint navigation, using a predefined waypoint list. It contains the position, desired altitude and speed with a waypoint command (take, loiter, land, etc.). It can be modified in flight using the Ground Control Station sofware called AirGuardian Virtual Cockpit.

4.1 Bearing Estimation

It is necessary to estimate the missing, and intermediate positions for the continuous bearing control (100 Hz – update frequency of the most actuators). This estimation can be computed using the yaw rate and the GPS bearing from the last valid NMEA sentence. The Z axis angular rate (Ψ – provided by the IMU) should be converted to heading turn rate ($\dot{\Psi}$) using the UAV bank angle [4]. With this procedure the actual bearing (θ_e) can be estimated between two valid GPS sentences using the last known bearing (θ) and $\dot{\Psi}$ (1). The heading angle provided by the IMU is often not reliable, because of the magnetic sensor used by the internal sensor fusion algorithms. This sensor is very sensitive to strong electromagnetic fields especially when the UAV has electric propulsion.

$$\theta_e = \theta + \dot{\Psi} \tag{1}$$

Small size (around 1 m wingspan) and small weight (under 2 kg) UAVs are quite agile so turn rates can reach high levels. For these airframes bearing estimation is essential.

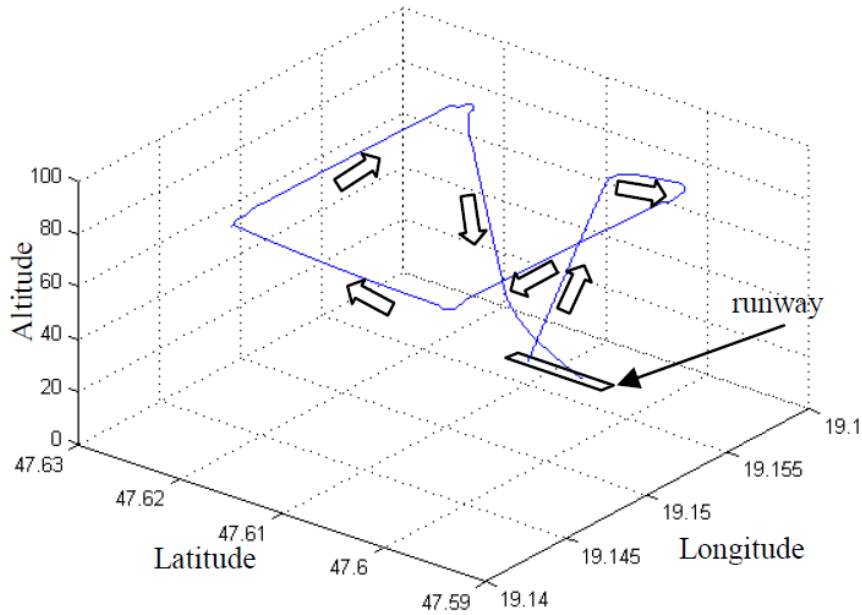

Figure 3. HIL simulated takeoff, cruise and landing with approach, glideslope and flare

4.2 Position Estimation

During the navigation, not only the bearing but also the position has to be estimated with a navigation Equations (2), (3), well known in nautical terms [5]. Unlike a complete inertial navigation system with minimal error [6, 7, 8] this system is using the GPS module as the main position sensor but makes it better. The estimation can be calculated from the SOG, estimated position and bearing (when known position and bearing are not available) using the earth radius R.

$$\mathrm{Lat}_2 = \mathrm{asin}(\sin(\mathrm{Lat}_1) \cdot \cos\left(\frac{d}{R}\right) + \cos(\mathrm{Lat}_1) \cdot \sin\left(\frac{d}{R}\right) \cdot \cos(\theta_e)) \tag{2}$$

$$\mathrm{Lon}_2 = \mathrm{Lon}_1 + \mathrm{atan2}(\sin(\theta_e) \cdot \sin\left(\frac{d}{R}\right) \cdot \cos(\mathrm{Lat}_1), \cos\left(\frac{d}{R}\right) - \sin(\mathrm{Lat}_1) \cdot \sin(\mathrm{Lat}_2)) \tag{3}$$

The travelled distance can be calculated from the estimated bearing and the estimated SOG which correlates with the local airflow. Usually there are 200 ms between two valid GPS sentence bursts, but the distribution of measured positions is not uniform. Even if one or two are corrupted the refresh time is always under

1 000 ms. Obviously there will be some errors, but usually they are low (under 1 m) and not causing any serious false position estimation. When there is no position fix due to a GPS error the bearing and position estimation method acts like an inertial navigation unit and the UAV can return home safely.

4.3 Vector Field Navigation

The vector field navigation calculates a desired bearing in every position, no matter what is the actual bearing of the UAV. This can be easily represented and understood as a vector field. The desired bearing (φ_d) depends on the position of UAV, bearing to destination waypoint (φ_T), route bearing (φ_R)) and the cross track error (D_{CT}) (Equations (4), (5), (6)) [9].

$$\delta = \sqrt[K_d]{|D_{CT} \cdot K_c \cdot (\varphi_T - \varphi_R)|} \cdot sign(D_{CT}) \quad (4)$$

$$\gamma = \min(1, D_T) \quad (5)$$

$$\varphi_d = \varphi_T + \delta * \gamma \quad (6)$$

The cross track error sensitivity can be set with Kc parameter and the path reaching smoothness with Kd. It is a common problem that the UAV misses the waypoint if the waypoint radius is low and there is a strong wind or the distance between the source and destination points is short. In this case the UAV turns back so the flight path will contain unnecessary loops. The first possibility to avoid this problem is the dynamic radius which must adapt to the local airflow characteristics. The other, and better solution is the usage of γ. If the UAV is close to the destination point (under 1 000 m) the parameter γ guarantees the reach of the waypoint, ignoring depending on the UAV – waypoint distance (Figure 4).

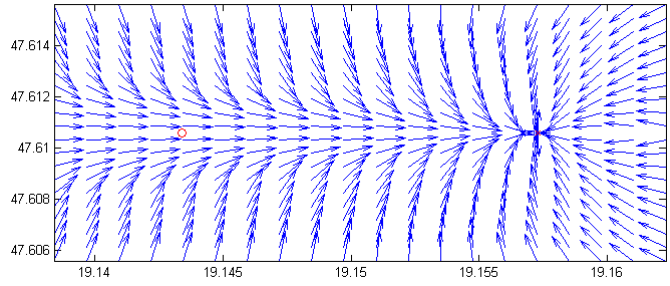

Figure 4. Vector field between source and destination waypoints

The first advantage of this navigation is the easy graphical setup of the internal parameters Kc ($\sim$ 10.0) and Kd ($\sim$ 0.5). The other is it has only one output parameter (ϕ_d) so nearly any controller type (such as third order non-linear, PID, fuzzy etc.) can suit this navigation because only the difference of desired and actual

bearing should be minimized. Furthermore, with a little modification – cross track error is measured as distance from radius (7), it is capable of loiter navigation over a desired position (Figure 5).

$$\varphi_d = \varphi_T + \frac{\pi}{2} + \min\left(|D_{CT} \cdot K_c|, \frac{\pi}{2}\right) \cdot \text{sign}(D_{CT}) \tag{7}$$

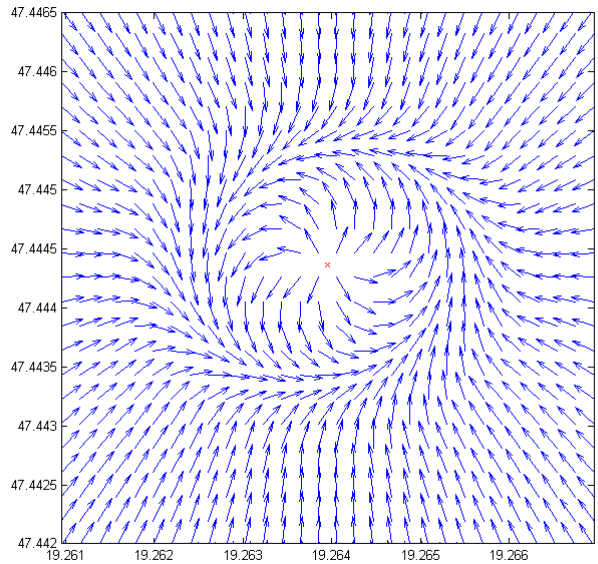

Figure 5. Loiter navigation

5 LANDING PREPARATIONS

During the flight, the aircraft is in motion in relation to the surrounding medium. This means the speed of the aircraft can be interpreted in the same way as in a ground vehicle in the case of calm weather when the medium is still. In the case of strong wind, the speed of the airflow is added to the airspeed of the aircraft. We measure the speed of the UAV with two different sensors with different principles. The first is the GPS, the second is the Pitot-Prandtl tube. The two measured values are the same in calm weather, but different in windy conditions. The difference of these values gives the wind speed at the current course. Measuring in 360 degrees with smooth resolution, we get the local wind direction and strength.

When the UAV mission and the landing position is near to the takeoff place, the local windmap can easily be computed during the flight. When the landing position

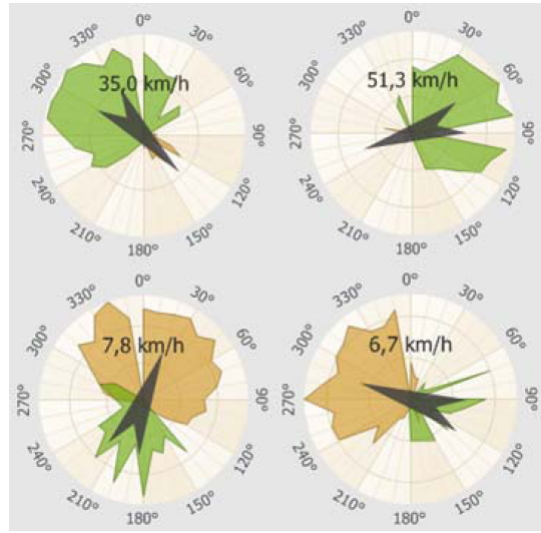

Figure 6. Wind maps in different weather conditions

is far away, after taking the last waypoint the UAV can compute the actual local wind parameters with a 360° turn before landing. With this information the autopilot can compute a pre-landing waypoint. From that assistant coordinate the UAV can glide to the desired landing position in headwind with an appropriate slope. There is no need for major direction correction because the wind blows frontwise and the slope angle is computed from the strength of the airflow; therefore the UAV can land precisely in the desired position. The process can also be used for parachute landing. It is a common problem that the aircraft is uncontrollable when the parachute is open. After the opening the UAV is drifted away by the wind and crashes on an obstacle. With the knowledge of the local airflow, parameters and optimal parachute opening position can be calculated to prevent dangerous situations.

A graphical representation can be plotted in a 0–360° polar coordinate system from the difference of the SOG and the airspeed (Figure 6). The measured values have to be stored in an array that covers the full 0–360 degree course range. For a faster calculation, the full range has to be divided into 36 pieces. Each piece is a FIFO buffer with length n. The data in the buffer has to be filtered with a slide window average filter method. The result is the average SOG – airspeed difference in every piece. In ideal case the absolute values of maximal differences are equal and their directions are roughly opposing. These values are only filling two quarters of the full polar coordinate system. The remaining quarters are representing wind data which is perpendicular to wind course. These are close to zero so they are negligible. The absolute value of average highest m measurement data of descending order sorted wind data is the current average wind speed. After converting each average SOG – airspeed difference to 36 vectors with neglection of the roughly zero ones

the positive and resultant vectors can be calculated. They give the dominant wind direction. If there are enough measurements from head and tailwind test flights the results are obvious. However, if the aeroplane is flying in a long straight course (no data in head and tailwind together) or there is not enough data for every direction, the result will be inaccurate. Another problem is the changing airflow direction, and the strong blasts which are difficult to eliminate.

Test flights have been repeated in different altitudes. Results showed the wind strength was stronger in higher altitude. It is a well known phenomenon which could be used to check the sensitivity and usefulness of the method. Of course, the flight tests could not indicate high altitude air flows but clearly showed the ground level ones. The higher the wind speed, the more possible to determine the current wind direction and speed. The measurement is hampered by the powerful wind blasts, which should be filtered, because they spoil it. In addition to these, measured data should be interpreted only within a given time because of weather changes.

6 TAKEOFF

Before takeoff the UAV must be programmed with the mission, including the route (with desired airspeed and altitude). The first waypoint is the home position, where the plane starts the takeoff. The remaining ones are mission specific. Usually small size UAVs are not using stated airfields or runways for takeoff. A small 50–100 m long 10–30 m wide clear field is enough for ground takeoff. In this case there is no visual exact border to perform a visual path following method. Only the GPS [10] and IMU can be used.

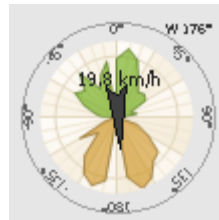

Figure 7. Windmap during test flight

The UAV should be in headwind when the Takeoff button is pressed. During the test flight there was a strong, 20 km/h (UAV cruising speed $\sim$ 50 km/h) headwind from the north (Figure 7). This command sets the takeoff direction and enables the engine. The throttle is at maximum, lateral axis is controlled by the elevator, lateral and longitudinal axis is with rudder and ailerons. After reaching full rpm the plane performs takeoff and starts climbing in a constant safe angle (Figure 8) until it reaches the safe altitude (usually 25 m). At this altitude the UAV switches to waypoint navigation, heading to the second waypoint (Figure 9), climbing to the desired waypoint altitude (usually 70–300 m for surveillance or photomapping). In

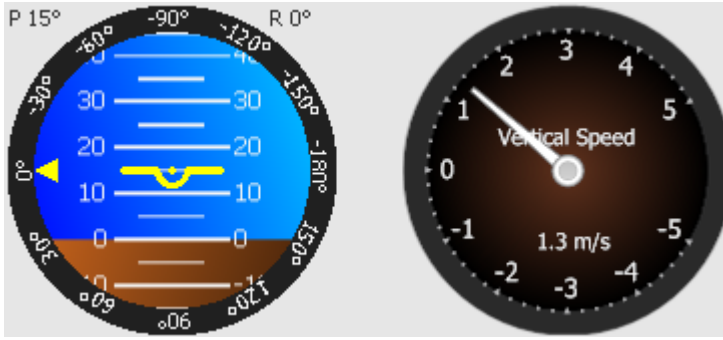

Figure 8. Test flight – 15 degree safe climb angle at takeoff with 1.3 m/s climb rate

waypoint navigation the airspeed is controlled by the elevator and the altitude with the throttle [18].

During takeoff the climbing angle can be controlled with classic PID or non-linear third order controller by the AERObot V5 autopilot.

7 LANDING

The landing must be performed in headwind for the best result. There are many robust, complex and precise landing methods [11, 12, 13, 14, 15] but for small size UAVs it is unnecessary. A much simpler, ILS like solution was developed, but without any additional onboard or ground hardware. The system works similarly to ILS guidance but the used control values are computed from GPS, IMU, barometric airspeed and altitude data (Figure 10).

7.1 Approach

After completing the mission the UAV approaches the landing zone. It can be the same as the takeoff or can be different. When is is not the same manual waypoint editing is required, otherwise they are calculated onboard based on home position and the used takeoff direction. After taking the last mission related waypoint, three landing related waypoints must be set. The first landing waypoint connects the flight path with the mission, the second sets the final heading to the landing zone and the approach altitude (Figure 11) to a lower value (e.g. 30 . . . 100 m).

During approach the flight controls are the same as in waypoint flight. Only the desired altitude is lower. The approach sets the final heading for landing.

7.2 Glideslope

After reaching the second landing waypoint the UAV performs the glideslope ($-10°$) path following maneuver (Figure 12). In this part of the landing the heading is

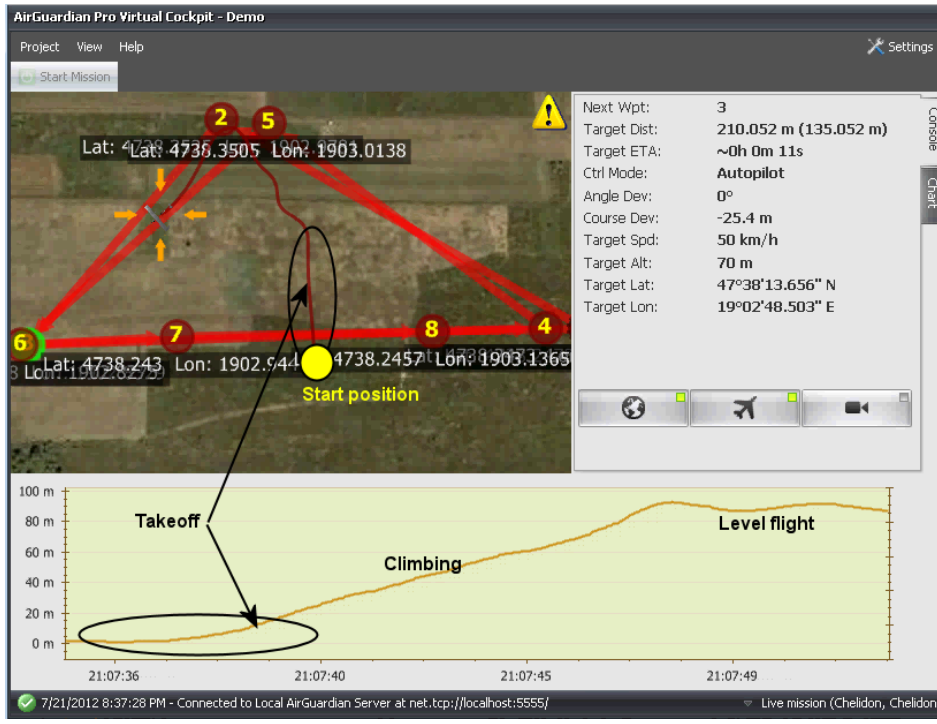

Figure 9. Test flight – takeoff in headwind

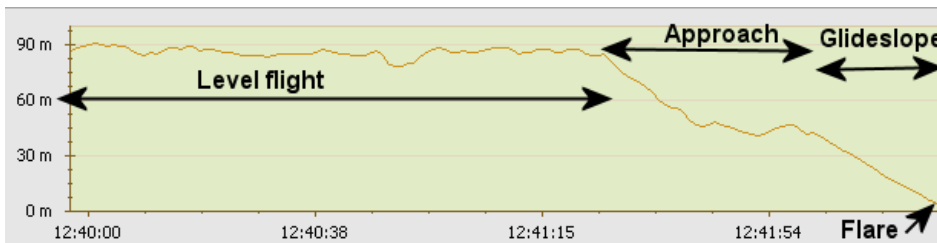

Figure 10. Test flight – landing altitude plot

controlled by the rudder and ailerons, the airspeed with the throttle and the altitude H_{desired} (using glideslope angle $\theta_{\text{glideslope}}$ and distance from landing waypoint $D_{\text{LandingWP}}$) with the elevator – similarly to takeoff (Equation (8)).

$$H_{\text{desired}} = \tan\theta_{\text{glideslope}} \cdot D_{\text{LandingWP}} \tag{8}$$

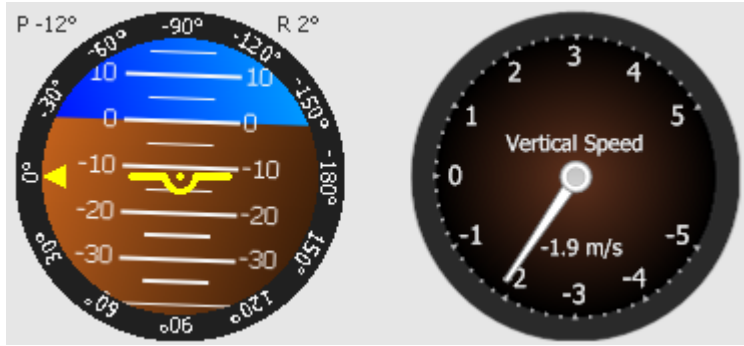

Figure 11. Test flight – approach angle and variometer

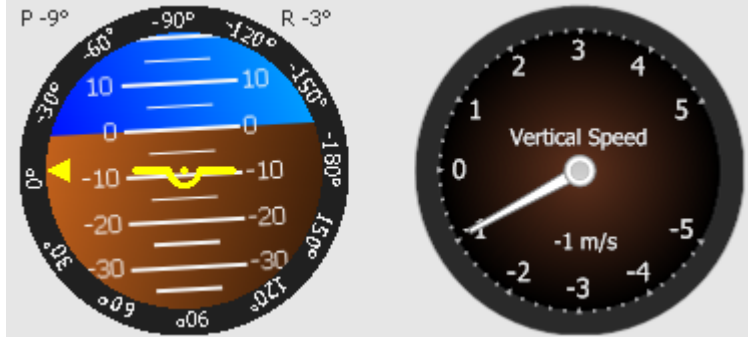

Figure 12. Test flight – −10° glideslope

7.3 Flare

When the UAV reaches a flare maneuver [16, 17] starting altitude (5–10 m) the autopilot stops the engine (zero throttle command for electric UAVs or throttle cut for internal combustion propulsion vehicles). In this very final stage there is no specific heading, altitude or airspeed control, only lateral, longitudinal and vertical stabilization with a certain amount of pitch angle (to slow the plane before touchdown).

8 CONCLUSIONS

A simple but preciese method was developed for small size UAVs for takeoff and landing which uses the onboard sensors without any additional onboard or ground hardware. The plane performs takeoff and starts climbing in a constant 15° angle with full throttle until it reaches a safe 25m altitude when the UAV switches to waypoint navigation, heading to the mission related waypoints.

The landing system works similarly to ILS guidance in commercial aviation but without any additional ground or onboard related guidance hardware. The used control values are computed from GPS, IMU, barometric airspeed and altitude data. During the takeoff, waypoint navigation and landing the vector navigation field was used.

Test results showed the system works the same as in simulation. Furthermore it is robust, works fine even in high (20 km/h – half the cruising speed of UAV) wind.

REFERENCES

[1] Roepcke, F.: ILS-Past and Present. In: Aerospace and Electronic Systems Magazine, IEEE, Vol. 5, 1990, No. 5, pp. 9–11.

[2] McFarland, R. H.: ILS – A Safe Bet for Your Future Landings. Aerospace and Electronic Systems Magazine, Vol. 5, 1990, No. 5, pp. 12–15.

[3] Stojcsics, D.: Flight Safety Improvements for Small Size Unmanned Aerial Vehicles. Proceedings of 16th IEEE International Conference on Intelligent Engineering Systems (INES 2012), June 13–15, 2012, Lisbon, Portugal, pp. 483–487, ISBN: 978-1-4673-2693-3 (pendrive); 978-1-4673-2692-6 (printed).

[4] Leven, S.—Zufferey, J.—Floreano, D.: A Minimalist Control Strategy for Small UAVs. In: Proc. IROS 2009, pp. 2873–2878.

[5] Ucan, F.—Altilar, D. T.: Navigation and Guidance Planning for Air Vehicles. In: Proceedings of 20th IEEE International Conference on Tools with Artificial Intelligence (ICTAI 2008), pp. 534–538.

[6] Li, Q.—Fang, Z.—Li, H.: The Application of Integrated GPS and Dead Reckoning Positioning. In: Automotive Intelligent Navigation System, Journal of Global Positioning Systems, Vol. 3, 2004, No. 1-2, pp. 183–190.

[7] Davidson, P.—Hautamki,J.—Collin, J.: Using Low-Cost MEMS 3D Accelerometers and One Gyro to Assist GPS Based Car Navigation System. In: Proceedings of 15th Saint Petersburg International Conference on Integrated Navigation Systems, May 2008.

[8] Zhao, L.—Ochieng, W. Y.—Quddus, M. A.—Noland, R. B.: An Extended Kalman Filter Algorithm for Integrating GPS and Low-Cost Dead Reckoning System Data for Vehicle Performance and Emissions Monitoring. Journal of Navigation, Vol. 56, 2003, pp. 257–275.

[9] Stojcsics, D.: Autonomous Waypoint Navigation Methods for Small Size Unmanned Aerial Vehicles. In: Acta Polytechnica Hungarica, Vol. 9, No. 4, ISSN 1785-8860 (to appear).

[10] Cho, A. et al.: Fully Automatic Taxiing, Takeoff and Landing of a UAV Using a Single-Antenna GPS Receiver Only. In: Proceedings of International Conference onControl, Automation and Systems, ICCAS 2007, pp. 821–825.

[11] Rui, W.—Zhou, Z.—Yanhang, S.: Robust Landing Control and Simulation for Flying Wing UAV. In: Proceedings of the 26th Chinese Control Conference 2007, pp. 600–604.

[12] Saini, G.—Balakrishnan, S. N.: Adaptive Critic Based Neurocontroller for Autolanding of Aircrafts. In: Proceedings of American Control Conference 1997, Vol. 2, pp. 1081–1085.

[13] Sprinkle, J.—Eklund, J. M.–Sastry, S. S.: Deciding to Land a UAV Safely in Real Time. In: Proceedings of American Control Conference 2005, pp. 3506–3511.

[14] Miele, A.—Wang, T.—Melvin, W. W.: Optimization and Guidance of Penetration Landing Trajectories in a Windshear. In: Proceedings of American Control Conference 1988, pp. 1428–1439.

[15] Singh, S.—Padhi, R.: Automatic Path Planning and Control Design for Autonomous Landing of UAVs Using Dynamic Inversion. In: Proceedings of American Control Conference (ACC '09), pp. 2409–2414.

[16] Serra, P.—Le Bras, F.—Hamel, T.—Silvestre, C.—Cunha, R.: Nonlinear IBVS Controller for the Flare Maneuver of Fixed-Wing Aircraft Using Optical Flow. In: Proceedings of 49th IEEE Conference on Decision and Control (CDC 2010), pp. 1656–1661.

[17] Kaminer, I.—Khargonekar, P. P.: Design of the Flare Control law for Longitudinal Autopilot Using H1 Synthesis. In: Proceedings of the 29th IEEE Conference on Decision and Control 1990, pp. 2981–2986.

[18] Molnár, A.—Stojcsics, D.: Fixed-Wing Small-Size UAV Navigation Methods with HIL Simulation for AERObot Autopilot. In: Proceedings of 9th International Symposium on Intelligent Systems and Informatics, Subotica, Serbia 8–10 Sept. 2011, ISBN: 978-1-4577-1975-2, pp. 241–245.

Dániel Stojcsics is a Ph. D. student at Óbuda University Budapest, Doctoral School of Applied Informatics. His main research area is in autonomous navigation and control of small size tailless UAVs.

András Molnár is an Associate Professor at buda University Budapest. He received his Ph. D. degree in 2005 at Zrínyi Miklós National Defence University. His main research area is in autonomous control of Unmanned Aerial Vehicles.